

## INFORMATION TO USERS

This dissertation copy was prepared from a negative microfilm created and inspected by the school granting the degree. We are using this film without further inspection or change. If there are any questions about the content, please write directly to the school. The quality of this reproduction is heavily dependent upon the quality of the original material.

The following explanation of techniques is provided to help clarify notations which may appear on this reproduction.

1. Manuscripts may not always be complete. When it is not possible to obtain missing pages, a note appears to indicate this.
2. When copyrighted materials are removed from the manuscript, a note appears to indicate this.
3. Oversize materials (maps, drawings and charts are photographed by sectioning the original, beginning at the upper left hand corner and continuing from left to right in equal sections with small overlaps.

**UMI**

ProQuest Information and Learning  
300 North Zeeb Road, Ann Arbor, MI 48106-1346 USA  
800-521-0600

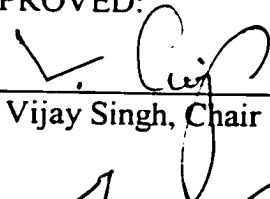
PREVIEW

CHARACTERIZATION OF JUNCTION TRANSPORT MECHANISMS  
IN CADMIUM TELLURIDE - CADMIUM SULFIDE  
THIN FILM PHOTOVOLTAIC DEVICES

DAVID L. LINAM

Department of Electrical and Computer Engineering

APPROVED:



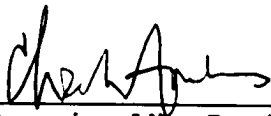
Dr. Vijay Singh, Chair



Dr. Gregory Lush



Dr. Jeff Drucker



Associate Vice President  
for Graduate Studies

## DEDICATION

To my wife Laurie and my daughter Lili.

PREVIEW

**CHARACTERIZATION OF JUNCTION TRANSPORT MECHANISMS  
IN CADMIUM TELLURIDE - CADMIUM SULFIDE  
THIN FILM PHOTOVOLTAIC DEVICES**

by

**David L. Linam, BSEE**

**THESIS**

**Presented to the Faculty of the Graduate School of**

**The University of Texas at El Paso**

**in Partial Fulfillment**

**of the Requirements**

**for the Degree of**

**Master of Science**

**Department of Electrical and Computer Engineering.**

**THE UNIVERSITY OF TEXAS AT EL PASO**

**May 2000**

## ABSTRACT

CdTe-CdS thin-film heterojunction photovoltaic devices fabricated at three different laboratories by close-space sublimation (CSS) have been characterized using electrical and optical techniques. Capacitance versus voltage (C-V) measurements were performed in the dark at temperatures between 200 Kelvin and 350 Kelvin. The current density versus voltage (J-V) characteristics of the cells were measured at temperatures between 200 Kelvin and 350 Kelvin in the dark and under broad-spectrum illumination intensities of approximately  $100\text{mW/cm}^2$  through  $100\mu\text{W/cm}^2$ . J-V characteristics were also studied using infrared (IR) illumination of various wavelengths. An analysis of the steady-state current settling time after a change in forward bias was performed. Additionally, dc quantum efficiency measurements were performed.

C-V data indicates the existence of a nearly intrinsic CdTe layer near the junction. C-V analysis and settling time measurements show that at least one and possibly many deep trap levels with large time constants in the CdTe layer affect the operational characteristics of the cells.

The J-V versus temperature and intensity data for the cells was fit to a parallel diode model that includes series and shunt resistance. Analyses of the extracted diode parameters reveal the existence of two junction transport mechanisms. The first is a depletion region recombination process that is independent of illumination intensity and active at high bias levels under low illumination intensities. The second mechanism is an intensity-dependent quantum mechanical tunneling transport mechanism that is active at

low bias levels and is significant under high illumination intensities. Quantum efficiency measurements and IR J-V analysis confirm that this tunneling transport is not active when the incident optical radiation is of energy less than the bandgap of CdTe.

A model of the CdTe-CdS solar cell as a p-i-n structure with a trap level in the CdTe layer is presented and analyzed. The C-V and settling time measurements agree well with predicted characteristics of the model. However, the p-i-n model cannot explain the observed tunneling transport characteristics.

PREVIEW

## TABLE OF CONTENTS

CHAPTER	PAGE
1 Introduction.....	1
2 Theory.....	3
2.1 Ideal CdTe-CdS heterojunction.....	3
2.2 Ideal solar cell theory.....	5
2.2.1 Energy band model for ideal solar cell.....	5
2.2.2 Single diode model for ideal solar cell.....	9
2.3 Effects of series and shunt resistance.....	10
2.4 Crossover.....	12
2.5 Junction transport mechanisms.....	12
2.5.1 Recombination currents.....	15
2.5.2 Tunneling currents.....	16
2.5.3 Interface states and bulk trap levels.....	18
2.6 Depletion capacitance.....	18
2.7 Illumination-dependent junction transport.....	21
2.8 Models for CdTe-CdS solar cell.....	21
2.8.1 Parallel diode model.....	21
2.8.2 Physical models.....	23
3 Experimental methods and materials.....	24
3.1 Device structure and fabrication.....	24



3.2	Steady-state settling time measurements.....	26
3.3	Capacitance versus voltage (C-V) measurements.....	27
3.4	Current density versus voltage (J-V) measurements.....	30
3.4.1	J-V measurement setup.....	30
3.4.2	J-V analysis.....	32
3.4.3	Infrared (IR) J-V measurements.....	36
3.5	Quantum efficiency measurements.....	36
4	Experimental results.....	38
4.1	C - V measurements.....	38
4.2	J - V measurements.....	49
4.3	IR J - V measurements.....	73
4.4	Quantum efficiency measurements.....	76
4.5	Settling time measurements.....	76
5	Discussion.....	79
5.1	The p-i-n model for CdTe-CdS solar cell.....	79
5.2	Discussion of experimental results.....	89
5.2.1	Discussion of C-V measurements.....	89
5.2.2	Discussion of settling time measurements.....	90
5.2.3	Discussion of J-V measurements.....	91
6	Conclusions.....	96
6.1	Conclusions.....	96
6.2	Future work.....	96

Appendix A	Derivation of capacitance correction formula.....	97
A.1	Derivation of correction formula for $C_p$ .....	97
A.2	Derivation of correction formula for $D$ .....	101
References	.....	103
<i>Curriculum Vitae</i>	.....	107

PREVIEW

## LIST OF TABLES

TABLE	PAGE
3.1 Data for the four CdTe-CdS solar cells studied in this work.....	26
3.2 Lamp voltage and filter usage for variable intensity J-V measurements.....	31

## LIST OF FIGURES

FIGURE	PAGE
2.1 Ideal CdTe-CdS heterostructure energy band diagram.....	4
2.2 Energy band diagrams illustrating operation of ideal solar cell.....	6
2.3 J versus V characteristics for ideal solar cell.....	8
2.4 $V_{OC}$ , $J_{SC}$ , $V_{MP}$ , and $J_{MP}$ for ideal solar cell.....	8
2.5 Single diode model of ideal solar cell.....	10
2.6 Effect of series and shunt resistance.....	11
2.7 Non-ideal “crossover” behavior of CdTe-CdS cell .....	13
2.8 Energy band diagrams showing junction transport mechanisms.....	14
2.9 Parallel diode model for CdTe-CdS solar cell.....	22
3.1 CdTe-CdS device structure.....	24
3.2 Setup for steady-state settling time measurement.....	26
3.3 Setup for capacitance versus voltage (C-V) measurement.....	28
3.4 Schematic of series resistance correction for capacitance measurements.....	29
3.5 Setup for current density versus voltage (J-V) measurement.....	30
3.6 Plot of $\ln(J_D)$ versus V showing the series resistance correction .....	35
3.7 Setup for quantum efficiency measurements.....	37
4.1 1MHz C-V data for cell M2 at various temperatures.....	39
4.2 1MHz C-V data for cell M3 at various temperatures.....	39
4.3 300 Kelvin C-V data for cell M2 at various frequencies.....	40

4.4	300 Kelvin C-V data for cell M3 at various frequencies.....	40
4.5	Frequency dependence of $d(1/C)/dV$ for cell M2.....	41
4.6	Frequency dependence of $d(1/C)/dV$ for cell M3.....	41
4.7	Extracted W versus V data for cell M2 at various frequencies.....	43
4.8	Extracted W versus V data for cell M3 at various frequencies.....	43
4.9	Extracted W versus V data for cell M2 at various temperatures.....	44
4.10	Extracted W versus V data for cell M3 at various temperatures.....	44
4.11	Extracted N versus W data for cell M2 at various frequencies.....	45
4.12	Extracted N versus W data for cell M3 at various frequencies.....	45
4.13	Extracted N versus W data for cell M2 at various temperatures.....	46
4.14	Extracted N versus W data for cell M3 at various temperatures.....	46
4.15	Extraneous state density for cell M2 at 300 Kelvin.....	47
4.16	Extraneous state density for cell M3 at 300 Kelvin.....	47
4.17	Extrapolated intrinsic region width for cell M2 at 300 Kelvin.....	48
4.18	Extrapolated intrinsic region width for cell M3 at 300 Kelvin.....	48
4.19	Plot of $\ln(J_D)$ versus V in the dark and at 1-sun for cell M1 at 350K.....	50
4.20	Plot of $\ln(J_D)$ versus V in the dark and at 1-sun for cell M1 at 300K.....	50
4.21	Plot of $\ln(J_D)$ versus V in the dark and at 1-sun for cell M1 at 250K.....	51
4.22	Plot of $\ln(J_D)$ versus V in the dark and at 1-sun for cell M1 at 200K.....	51
4.23	Plot of $\ln(J_D)$ versus V at various intensity levels for cell M2 at 350K.....	52
4.24	Plot of $\ln(J_D)$ versus V at various intensity levels for cell M2 at 300K.....	52
4.25	Plot of $\ln(J_D)$ versus V at various intensity levels for cell M2 at 250K.....	53

4.26	Plot of $\ln(J_D)$ versus $V$ at various intensity levels for cell M2 at 200K.....	53
4.27	Plot of $\ln(J_D)$ versus $V$ at various intensity levels for cell M3 at 350K.....	54
4.28	Plot of $\ln(J_D)$ versus $V$ at various intensity levels for cell M3 at 300K.....	54
4.29	Plot of $\ln(J_D)$ versus $V$ at various intensity levels for cell M3 at 250K.....	55
4.30	Plot of $\ln(J_D)$ versus $V$ at various intensity levels for cell M3 at 200K.....	55
4.31	Plot of $\ln(J_D)$ versus $V$ parallel diode curve fits for cell M2 at 350K.....	57
4.32	Plot of $\ln(J_D)$ versus $V$ parallel diode data and curve fits for cell M2 at 350K.....	57
4.33	Plot of $\ln(J_D)$ versus $V$ parallel diode curve fits for cell M2 at 300K.....	58
4.34	Plot of $\ln(J_D)$ versus $V$ parallel diode data and curve fits for cell M2 at 300K.....	58
4.35	Plot of $\ln(J_D)$ versus $V$ parallel diode curve fits for cell M2 at 250K.....	59
4.36	Plot of $\ln(J_D)$ versus $V$ parallel diode data and curve fits for cell M2 at 250K.....	59
4.37	Plot of $\ln(J_D)$ versus $V$ parallel diode curve fits for cell M2 at 200K.....	60
4.38	Plot of $\ln(J_D)$ versus $V$ parallel diode data and curve fits for cell M2 at 200K.....	60
4.39	Plot of $\ln(J_D)$ versus $V$ parallel diode curve fits for cell M3 at 350K.....	61
4.40	Plot of $\ln(J_D)$ versus $V$ parallel diode data and curve fits for cell M3 at 350K.....	61
4.41	Plot of $\ln(J_D)$ versus $V$ parallel diode curve fits for cell M3 at 300K.....	62
4.42	Plot of $\ln(J_D)$ versus $V$ parallel diode data and curve fits for cell M3 at 300K.....	62
4.43	Plot of $\ln(J_D)$ versus $V$ parallel diode curve fits for cell M3 at 250K.....	63
4.44	Plot of $\ln(J_D)$ versus $V$ parallel diode data and curve fits for cell M3 at 250K.....	63
4.45	Plot of $\ln(J_D)$ versus $V$ parallel diode curve fits for cell M3 at 200K.....	64
4.46	Plot of $\ln(J_D)$ versus $V$ parallel diode data and curve fits for cell M3 at 200K.....	64
4.47	Plot of $\ln(J_D)$ versus $V$ curve fits for cell M1 at various temperatures.....	65

4.48	$J_{0B}$ versus intensity and temperature for cell M2.....	66
4.49	$J_{0B}$ versus intensity and temperature for cell M3.....	66
4.50	Plot of $\alpha_B$ versus temperature for cells M2 and M3.....	67
4.51	Series resistance versus intensity and temperature for cell M1.....	67
4.52	Series resistance versus intensity and temperature for cell M2.....	68
4.53	Series resistance versus intensity and temperature for cell M3.....	68
4.54	Shunt resistance versus intensity and temperature for cell M2.....	69
4.55	Shunt resistance versus intensity and temperature for cell M3.....	69
4.56	$J_{0A}$ versus temperature for cells M1, M2, and M3.....	71
4.57	Diode ideality factor versus temperature for cells M1, M2, and M3.....	71
4.58	$J_{00}$ and $\Delta E$ for cells M1, M2, and M3.....	72
4.59	$J_{00}$ and $\Delta E$ for cells M1, M2, and M3 (using high temperature data).....	72
4.60	IR response at $\lambda = 850\text{nm}$ for cell M2.....	74
4.61	IR response at $\lambda > 1\mu\text{m}$ for cell M2.....	74
4.62	IR response at $\lambda = 850\text{nm}$ for cell M3.....	75
4.63	IR response at $\lambda > 1\mu\text{m}$ for cell M3.....	75
4.64	Quantum efficiency for cell M2 and M3.....	77
4.65	Settling time for cell M2 in the dark.....	77
4.66	Settling time for cell M3 in the dark.....	78
5.1	Model of p-i-n CdTe-CdS heterojunction at thermal equilibrium.....	80
5.2	Model of p-i-n CdTe-CdS heterojunction under small forward bias.....	81

5.3	Model of p-i-n CdTe-CdS heterojunction under large forward bias.....	82
5.4	Detail of p-i-n model energy band diagram near the CdTe-CdS junction.....	86
A.1	Schematic of circuit used in series resistance correction of C-V data.....	97

PREVIEW



## CHAPTER 1

### INTRODUCTION

A photovoltaic device, or solar cell, is a semiconductor device that converts solar radiation directly into electricity. Because of the depletion rate of fossil fuels and the expense and safety concerns associated with nuclear power sources, cleaner renewable energy sources will be needed in the future to meet the world's growing energy needs [1]. Solar cells are being extensively researched because of the virtually limitless supply of solar energy, the achievement of high conversion efficiency, low operating cost, and almost pollution-free operation. Currently, solar cells are used for a variety of scientific and commercial applications, including power generation for spacecraft and satellites, commercial power generation in remote areas where the cost of installing power generation and transmission lines is prohibitive, and power for handheld consumer electronics.

The single-crystal silicon solar cell has been extensively used for a variety of applications, but the production costs associated with this type of device limits its application for widespread commercial use. Low cost alternatives, such as thin-film and polycrystalline devices, promise a more cost-effective alternative [1,2]. Thin-film Cadmium Telluride (CdTe)-Cadmium Sulfide (CdS) heterojunction solar cells have been studied for years [3-18] because of the nearly ideal bandgap energy of CdTe for solar absorption and the lower production costs promised by thin film devices [3].

The solar spectral radiation reaching the earth near the equator at midday is referred to as “one sun” illumination and has a power density of approximately  $100\text{mW/cm}^2$  [2]. The spectral intensity of this radiation can be approximated by a 5800K blackbody, although the earth’s atmosphere attenuates certain wavelengths. A semiconductor is transparent to radiation of lower energy than the semiconductor’s bandgap ( $hc/\lambda < E_g$ ) [1]. Additionally, the open-circuit voltage of a solar cell is limited by several factors, including bandgap energy. Assuming ideal conversion efficiency, the optimum bandgap for a semiconductor solar cell is about 1.5eV [1,2]. This makes CdTe ( $E_g \approx 1.5\text{eV}$ , direct) [2] a nearly ideal semiconductor for absorption of solar radiation.

Although high efficiencies have been achieved with CdTe-CdS thin film solar cells [12,13,15], higher efficiencies are at least theoretically possible [15]. Improvements in efficiency will undoubtedly come about with a deeper understanding of the non-ideal behavior of these devices, partially caused by interface states and deep trap levels associated with polycrystalline semiconductors.

The purpose of this work is to characterize the dark current transport mechanisms in several CdTe-CdS photovoltaic devices with various efficiencies, fabricated by different methods at different laboratories. An attempt is made to explain the operational characteristics in terms of existing physical models, and modify those models where appropriate to account for observed behaviors.

## CHAPTER 2

### THEORY

#### 2.1 Ideal CdTe-CdS heterojunction

A heterojunction is formed when two dissimilar semiconductors are brought into contact. Heterojunction theory is based on the work of Anderson [19], and is described elsewhere [2]. Figure 2.1 depicts the energy band diagram of a p-CdTe/n-CdS heterojunction with no deep trap levels, or interface states before and after joining. In the diagram,  $\chi$  is the electron affinity of the semiconductor,  $E_g$  is the bandgap energy of the semiconductor, and  $\Delta E_C$  and  $\Delta E_V$  are the conduction band and valence band discontinuities, respectively, given by:

$$\Delta E_C = \chi_p - \chi_n \quad (2.1)$$

$$\Delta E_V = E_{gn} - E_{gp} - \Delta E_C \quad (2.2)$$

If  $\Delta E_C$  is positive or  $\Delta E_V$  is negative then spikes in the conduction or valence band may be present which would impede the flow of charge across the junction. For the ideal CdTe-CdS heterojunction described here,  $\Delta E_C = -0.22\text{eV}$  and  $\Delta E_V = 1.2\text{eV}$  so there should be no spikes present in the CdTe-CdS junction. The diffusion potential at the junction is given as

$$V_d = V_{dn} + V_{dp} = \frac{1}{q} (E_{gp} - \delta_p - \delta_n + \Delta E_C). \quad (2.3)$$

The relative voltage supported in each semiconductor is

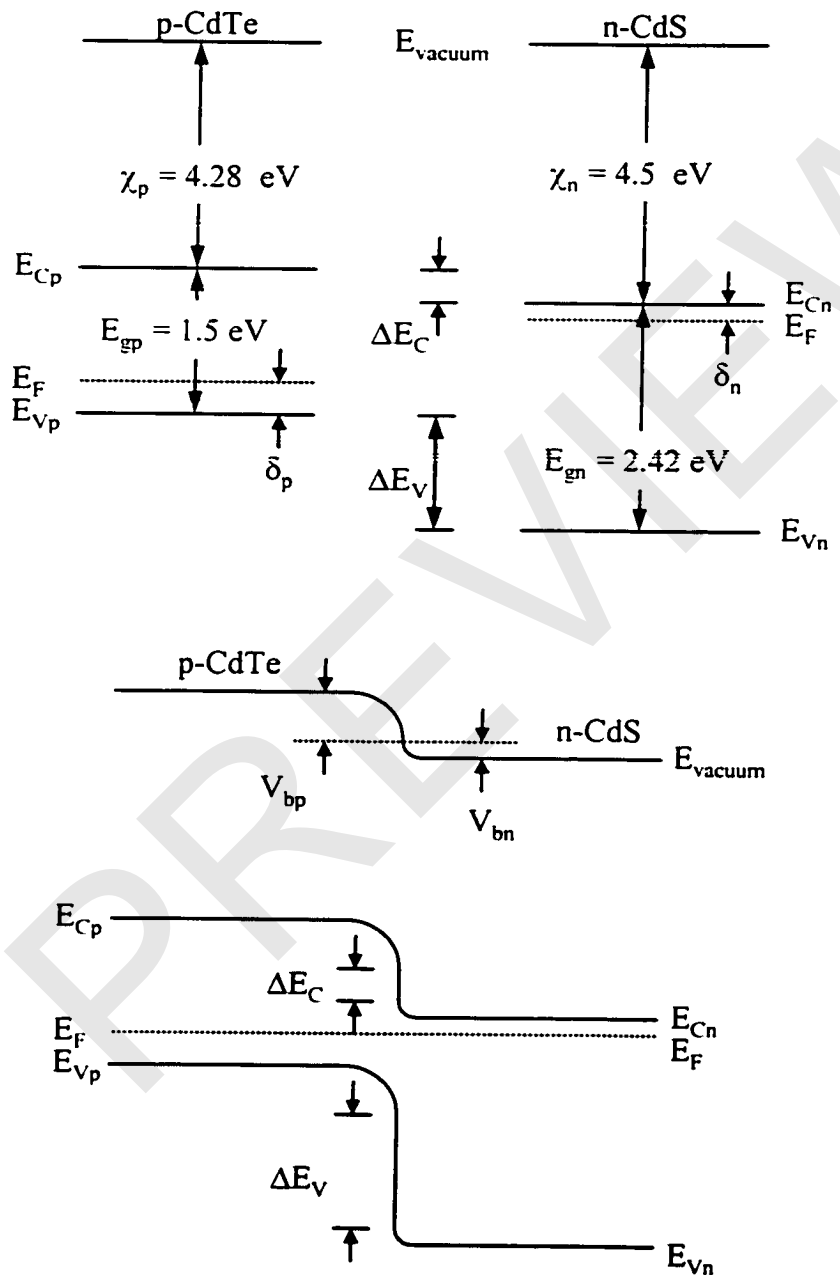


Figure 2.1 Energy band diagram of ideal CdTe-CdS heterojunction before and after joining.

$$\frac{V_{dn}}{V_{dp}} = \frac{V_n}{V_p} = \frac{N_A \epsilon_p}{N_D \epsilon_n}, \quad (2.4)$$

where  $V = V_n + V_p$  is the applied voltage across the semiconductor and  $V_p$  and  $V_n$  are the portions of the applied voltage dropped on the p-side and n-side of the junction, respectively.

## 2.2 Ideal solar cell theory.

### 2.2.1 Energy band model for ideal solar cell.

A solar cell is a semiconductor p-n junction that is optimized for conversion of solar radiation into electricity. For the ideal solar cell presented here, the device is assumed to be an abrupt p-n homojunction. A brief description of the device operation is given here, and a more thorough treatment of the subject is given in the literature [1,2].

Figure 2.2 depicts the energy band diagram of an ideal solar cell under illumination at  $V = 0$  (short circuit) (Fig. 2.2a) and at  $V = V_{OC}$  (open circuit) (Fig. 2.2b). When an ideal solar cell is illuminated, photons with energy greater than the bandgap energy  $E_g$  are absorbed creating electron-hole pairs. If the electron-hole pairs are created within a diffusion length of the junction, the minority carriers (electrons in the p-type material and holes in the n-type material) will diffuse to the space charge region before recombining and will be swept across the junction by the electric field. This light-generated current ( $J_L$ ) is assumed to be independent of bias voltage. When the junction is forward biased, the potential barrier is lowered, enabling minority carriers to diffuse across the junction. The resulting current is the sum of the electron forward current and

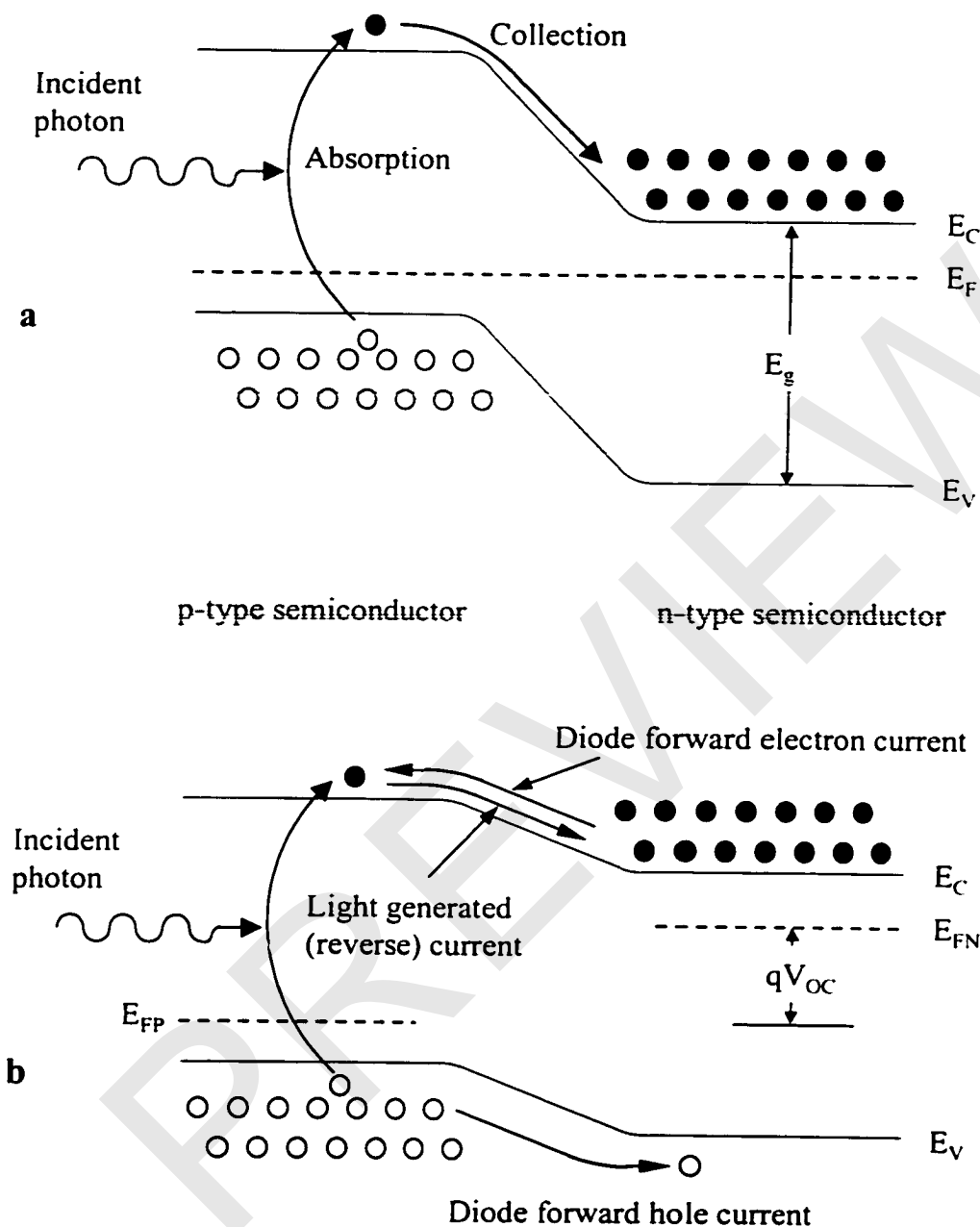


**Figure 2.2** Energy band diagram showing ideal solar cell operation in (a) short circuit condition ( $V_F = 0V$ ), and (b) open circuit condition ( $V_F = V_{OC}$ ).

the hole forward current and flows in the opposite direction to the light-generated current.

This diode current is called the dark current ( $J_D$ ) and is described by [1]

$$J_D = J_0 \left[ \exp\left(\frac{qV}{kT}\right) - 1 \right], \quad (2.5)$$

where  $q$  is the electron charge,  $k$  is Boltzman's constant, and  $T$  is the temperature in Kelvin.  $J_0$  is the diode reverse saturation current density and is given as

$$J_0 = \frac{qD_p p_{n0}}{L_p} + \frac{qD_n n_{p0}}{L_n}, \quad (2.6)$$

where  $n_{p0}$  ( $p_{n0}$ ) is the equilibrium minority electron (hole) concentration,  $D_n$  ( $D_p$ ) is the electron (hole) diffusion coefficient, and  $L_n$  ( $L_p$ ) is the electron (hole) diffusion length.

The temperature dependence of the reverse saturation current density may be approximated by [1]

$$J_0 \approx J_{00} \exp\left(\frac{-E_g}{kT}\right), \quad (2.7)$$

where  $J_{00}$  is weakly temperature dependent.

For the ideal device, superposition holds and the resulting current versus voltage (J-V) characteristics are shown graphically in Fig. 2.3 for the device in the dark and under illumination. Note that, for the ideal case, the two curves are identical except for the vertical shift caused by the light-generated current.

If the illuminated cell is biased at a point occurring in quadrant four, power can be extracted from the device. The bias point at which delivered power is maximized is known as the maximum power point where  $V=V_{MP}$  and  $J=J_{MP}$ . These points are depicted

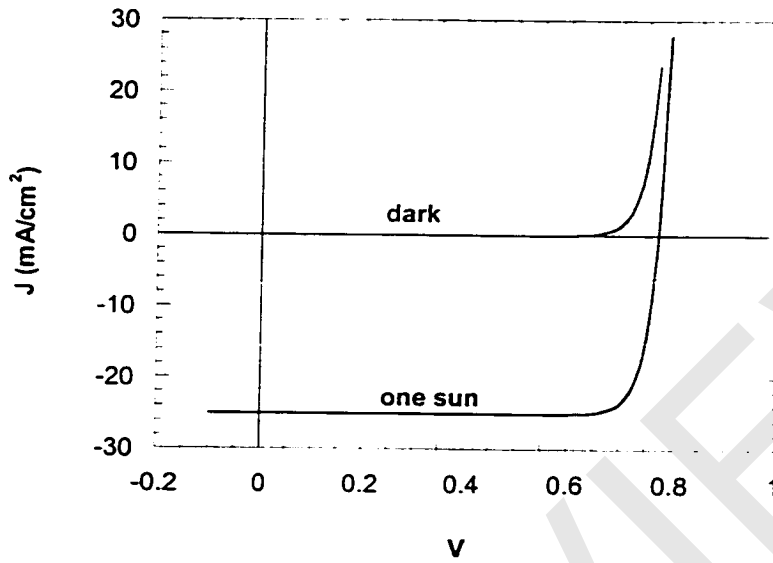


Figure 2.3  $J$  versus  $V$  characteristics for ideal solar cell.

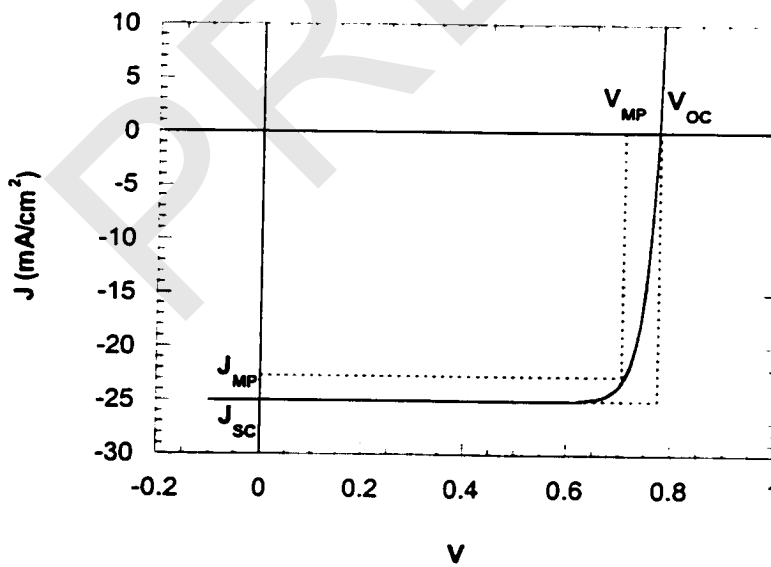


Figure 2.4  $V_{OC}$ ,  $J_{SC}$ ,  $V_{MP}$ , and  $J_{MP}$  for ideal solar cell.